Visualization-aided NIMBUS-based Multi-Criteria Decision-Making Using Interpretable Self-Organizing Maps (iSOM)

Deepanshu Yadav*, Deepak Nagar*, Palaniappan Ramu*, and Kalyanmoy Deb†, *Fellow, IEEE*
*Department of Engineering Design, Indian Institute of Technology, Madras, India
†Department of Electrical and Computer Engineering, Michigan State University, East Lansing, USA

COIN Report Number 2022016

***Abstract*—In multi-criterion optimization, often decision-makers (DMs) are not interested in the complete Pareto-optimal front. Instead, they have preferences that favor specific parts of the Pareto-optimal front. Besides looking for a specific trade-off among objectives, DMs are also interested in certain properties of solutions, such as away from constraint surfaces, Pareto-set boundaries, etc. Multi-criterion decision-making (MCDM) literature provides a plethora of approaches to introduce DM's preference information interactively to solve multi-criterion optimization problems. Often, interactions with DMs can be aided by a user-friendly visualization method or by using special data analysis procedures. An earlier study has indicated the use of self-organizing maps (SOM) as a tool for analyzing Pareto-optimal solutions. In this paper, we demonstrate how a specific MCDM method – NIMBUS – can be applied with the interpretable SOM (iSOM) approach iteratively to arrive at one or more preferred solutions in a multi-criterion optimization problem. The two-dimensional iSOM cells are marked with different colors and styles to indicate various properties of solutions- feasible and infeasible solutions, cluster boundaries, selected region for the NIMBUS-based search, starting, alternate, intermediate and final solutions. A visual illustration of the entire high-dimensional search space into a reduced two-dimensional space allows DMs to have a better understanding of the interactions of the objectives and constraints variable-wise and to execute NIMBUS decision-making procedure in a well-informed manner. The paper demonstrates the proposed method for several multi- and many-objective numerical and engineering problems. The approach is now ready to be applied to demonstrate the working of other popularly-used MCDM methods.**

***Index Terms*—multi-criteria decision making, NIMBUS, SOM, Pareto optimal front, multi-criterion optimization.**

I. Introduction

Optimization problems are now being increasingly solved for more than one criterion for several reasons. First, most practical problems are better posed as a multi-criterion optimization problem, as often the resulting optimal solution(s) must conform to several conflicting functional goals (such as cost, quality, emission, waste, etc.). Second, despite the ultimate choice of a single preferred optimal solution, multiple trade-off optimal solutions, which become the outcome of a multi-criterion optimization problem, provide a relevant knowledge of possible alternate solutions to the decision-makers (DMs) for them to be on top of guesses and prejudices. Finding a set of trade-off optimal solutions (known as Pareto-optimal solutions in the parlance of multi-criterion optimization) has mostly been followed using two broad philosophies of optimization: (i) generative approach [1], [2], [3] in which a single Pareto-optimal solution is found one at a time by solving a parameterized scalarization of multiple criteria and (ii) simultaneous approach [4], [5] in which multiple Pareto-optimal solutions are found in a single run of the algorithm. Evolutionary Multi-objective Optimization (EMO) methodologies, proposed in the early nineties fall in the second category of algorithms, which are now being extended to solve up to 15 objective problems routinely [6], [7].

In addition to optimization algorithms to find multiple Pareto optimal solutions, there is a need for multi-criterion decision-making (MCDM) task which can follow the optimization task or be applied interactively with the optimization task [8]. Starting in the early seventies, various MCDM approaches were proposed to systematically involve one or more DMs in providing preference information, either in terms of objective preferences irrespective of solutions, preference of one solution over another in a pairwise comparison based on their objective and constraint values, or by other means. These interactive MCDM approaches usually formulate a scalarized version of the multi-criterion optimization problems in an interactive manner. The scalarization process requires DM's preference information and thereby largely depends on the solutions being compared and their properties. To properly formulate a scalarized problem, it is extremely helpful to the DMs to visualize the solutions well in a low-dimensional mapped search space along with trade-off information of objectives, their nearness to constraint boundaries, and other relevant information assisting in the decision-making process. It is needless to say that an efficient decision-making process is less likely to be completely algorithmic; rather, it should be as procedural as possible but must accompany different analysis tools providing relevant trade-off information, but importantly it must be guided by human decision-makers having a direct stake in the problem [9].

Thus, it is clear from the above discussion that a multi-criterion problem-solving task cannot be a pure algorithmic exercise of finding just any optimal solution in the search space, but must involve human decision-makers, their perception of solutions through preferences of objectives and constraints involved in the problem [10]. The latter task can be aided by a proper understanding of the location of key solutions in the search space, the trade-off they produce among objectives and their closeness to constraint boundaries. This decision-making task can be better achieved through the use of modern data analysis and visualization methods that are easily understandable to human decision-makers. This paper demonstrates such an aspect of decision-making on a popularly used MCDM

approach using a recent data analysis and visualization tool on several three to five-objective problems.

There exist many systematic MCDM methods for achieving the optimization and decision-making tasks together. The use of an aspiration objective point and a preference direction vector in the Achievement Scalarization Function (ASF) approach [11], [12] is used to scalarize multiple objectives into a single objective, thereby producing a single optimal solution in the end. ASF and its augmented version (AASF) [13] are extensively used to develop a number of MCDM methods, such as, surrogate worth trade-off (SWT) method [14], [15], GUESS method [16], satisficing trade-off method (STOM) [17], Pareto-race method [18], [19], and others. These methods systematically change either the aspiration point or the preference direction vector in an iteration depending on the solution obtained at the previous iteration. Some of these systematic approaches are integrated with EMO methods mainly to find more than one preferred Pareto-optimal solution in the vicinity of the Pareto-optimal solution of the scaralized problem to provide some flexibility in choosing a different alternate but preferred solution. On some occasions, EMO methods were shown to apply a specific MCDM approach parallelly from multiple preferred solutions as a further process of providing flexibility in the scalarization process. Reference point-based NSGA-II (R-NSGA-II) [6], reference direction-based NSGA-II [20], light beam approach [21], [22] are some such hybrid EMO-MCDM methods. The implementation of interactive approaches using other MCDM techniques is recently studied in [23], [24].

The Non-differentiable Interactive Multiobjective BUndle-based optimization System (NIMBUS) is another interactive multi-criterion optimization and decision-making approach proposed in [25] and is the focus of this paper. It starts with a single Pareto-optimal solution and works iteratively to arrive at another preferred Pareto-optimal solution satisfying DM's satisfaction level on different objectives and constraints. At each iteration, the DM can classify all conflicting objectives into five classes, each indicating different levels of their satisfaction. For example, certain objectives may require to be improved further from their values at the current solution, or certain objectives may be allowed to deteriorate within specific limits for the improvement of some other objectives to take place, or certain objectives can be changed to any extent possible, as in the present context, they are not as important as the former two classes, and so on. Once such preference information is provided by the human DMs based on their desire and perception of an acceptable solution, scalarized single-objective formulation/s of the problem are formulated and solved to find an alternative solution. A feasibility check is always enforced to produce feasible solutions. The new solutions are compared with the previous solution(s), and a single solution is chosen to advance to the next iteration. The process is terminated when the DMs have found a satisfactory solution or a pre-defined number of iterations are elapsed.

It is clear from the above discussion that the progress of the entire process depends on DM's classification of objectives into different classes and the choice of a solution among a few at the end of each iteration. While there is no absolute right or wrong answer to this decision-making process, the DMs can be aided with adequate problem-related information with an easy-to-understand visualization tool to make a proper choice. A recent study [26] by the author group has shown that an interpretable version of self-organizing maps (they named the procedure as 'iSOM') can produce a series of two-dimensional SOM plots of each objective and constraint function in two fictitious mapped axes of the entire n-dimensional search space. The SOM plots are called the component planes of the respective variables, objectives, or constraints. The objective/constraint values are shown in small hexagonal (or rectangular) colored cells indicating their values. Since the axes are kept invariant for each objective/constraint SOM plot, a good idea of the trade-off among objectives can be perceived by traversing in certain fixed directions on two or more SOM plots. Moreover, the SOM plots provide a clear direction of maximal increase and decrease of each function value, thereby allowing one to investigate of the change in other function values along the fixed directions to get a good idea of trade-off among objectives and constraints.

In this paper, we take NIMBUS start point and show it on iSOM component planes to provide a clear understanding of the start point in the entire search space. This allows the DMs to have a better understanding of trade-off of objectives and constraints, so they are in a more informed position to provide classification levels of objectives and visualize the part of Pareto front obeying the classification, which is the region of interest (RoI) as well. iSOM visualization aids to select alternate solutions, generate intermediate solutions, and choose the final solution, knowing fully the scope of feasible solutions and RoI. In addition, the DMs are provided with the previous iteration's NIMBUS solutions on the same iSOM component planes to have a clear idea of their relative importance to progress to the next iteration. Since the iSOM procedure is agnostic to the actual variable space dimension and plots are always shown in two dimensions, they are relatively easy to comprehend. Moreover, our proposed iSOM component planes use different innovative fills and colors of hexagonal cells to make the whole process attractive and easier to use, a matter which is not possible to achieve with existing visualization methods.

In the remainder of this paper, we provide a brief description of the NIMBUS method in a step-by-step format in Section II and emphasize the need for using an effective visualization method to accompany its iterative steps. Then in Section III, we provide a brief description of the iSOM procedure. The overall procedure of iSOM-based visualization for NIMBUS method is provided in step-by-step format with details of color and style coding in Section IV. The advantages of using the iSOM-NIMBUS procedure compared to existing methods are highlighted in Section V in the context of a real-world three-objective crash-worthiness problem. Thereafter, the iSOM-NIMBUS procedure is further applied to different benchmark problems (five-objective problem, disjointed Pareto-set problem, and constrained problem) in Section VI. Finally, iSOM-NIMBUS is applied to two more real-world problems in Section VII. Conclusions of this extensive study is then summarized in Section VIII.

II. NIMBUS ALGORITHM

NIMBUS refers to Non-differentiable Interactive Multiobjective BUndle-based optimization System. As the name suggests, it is a multiobjective optimization (MOO) system that is able to handle even non-differentiable functions [27], [28]. However, the assumptions behind the implementation of NIMBUS are that all objective functions and constraint functions are locally Lipschitz continuous and that the feasible region $\{\mathbf{x} \in \mathbb{R}^n |\ \mathbf{g(x)} \leqslant 0\}$ is convex [29]. ($\mathbf{x}$ is the vector of the design variable and $\mathbf{g(x)}$ is the set of constraints functions). Given the MOO problem:

$$\begin{aligned} \underset{(\mathbf{x})}{\text{Minimize}} \quad & \big\{f_1(\mathbf{x}), \ldots, f_M(\mathbf{x})\big\}, \\ \text{subject to:} \quad & \mathbf{g(x)} = \big(g_1(\mathbf{x}), \ldots, g_J(\mathbf{x})\big)^T \leqslant 0, \end{aligned} \tag{1}$$

where $\mathbf{f(x)} = \big\{f_1(\mathbf{x}), \ldots, f_M(\mathbf{x})\big\}^T$ is a vector of objective functions. NIMBUS is based on the classification of the objective functions f_i into the following five classes [28], based on the objective vector $\mathbf{f}(\mathbf{x}^h)$ at the current solution $\mathbf{x}^h$, as follows:

1) whose values should be minimized further requiring $f_i(\mathbf{x}) < f_i(\mathbf{x}^h)$, for $i \in I^<$,
2) whose values should be minimized till some aspiration level $\bar{z}_i$ ($< f_i(\mathbf{x}^h)$), such that $f_i(\mathbf{x}) \geqslant \bar{z}_i$ for $i \in I^\leqslant$,
3) whose current values are satisfactory at the moment ($i \in I^=$),
4) whose values are allowed to increase until or up to a specific upper bound ε_i ($\geqslant f_i(\mathbf{x}^h)$), such that $f_i(\mathbf{x}) \leqslant \varepsilon_i$ for $i \in I^\geqslant$, and
5) whose values can change freely ($i \in I^{<>}$).

The difference between the classes $I^<$ and $I^\leqslant$ is that the functions in the former class are to be minimized as far as possible, as the functions in the latter class are to be minimized only till the aspiration level. At each iteration, the DM has the option to classify the objective functions at a feasible start point/current solution. Based on the classification a new (multiobjective) optimization problem is formed and solved by *Multiobjective Proximal Bundle* (MPB) method [29].

The authors of the NIMBUS method have changed the formulation of the scalarization problem many times since their first study [30], but the one shown below [31] guarantees finding a Pareto-optimal solution. Let $f(\mathbf{x}^h)$ be the feasible start point at an iteration, at which the classification is performed. Further to the classification, the following augmented achievement scalarizing function (AASF) sub-problem is formulated:

$$\begin{aligned} \underset{(\mathbf{x})}{\text{Minimize}} \ & \max_{i \in I^<, j \in I^\leqslant} \left[\frac{f_i(\mathbf{x}) - z_i^*}{z_i^{\text{nad}} - z_i^{**}}, \frac{f_j(\mathbf{x}) - \bar{z}_j}{z_j^{\text{nad}} - z_j^{**}}\right] + \rho \sum_{i=1}^{M} \frac{f_i(\mathbf{x})}{z_i^{\text{nad}} - z_i^{**}}, \\ \text{subject to:} \ & f_i(\mathbf{x}) \leqslant f_i(\mathbf{x}^h), \quad i \in I^< \cup I^\leqslant \cup I^=, \\ & f_i(\mathbf{x}) \leqslant \varepsilon_i, \quad i \in I^\geqslant, \\ & \mathbf{g(x)} = (g_1(\mathbf{x}), \ldots, g_m(\mathbf{x}))^T \leqslant 0, \end{aligned} \tag{2}$$

where, z_i^{nad} and z_i^* are nadir and ideal objective values, respectively, of the i-th objective, and z_i^{**} (slightly smaller than z_i^*) is the utopian objective value. These values are computed at the start of the NIMBUS procedure. While it is possible to obtain the ideal objective vector by minimizing each constrained objective function individually, the nadir objective vector can only be estimated [32]. The parameter ρ is usually chosen to be a small value ($\approx 10^{-3}$) and the term including ρ ensures that the resulting optimal solution of the above problem is a Pareto-optimal point, and not a weak Pareto-optimal point [1].The denominators in the terms of the objective function control the reference direction for the AASF formulation.

[29] also proposed the use of following three more sub-problem formulations to find *alternate* solutions using other standard MCDM approaches. In the next sub-problem, the scalarizing function used is the satisficing trade-off method (STOM, [17]):

$$\begin{aligned} \underset{(\mathbf{x})}{\text{Minimize}} \quad & \max_{i=1,\ldots,M} \left[\frac{f_i(\mathbf{x}) - z_i^{**}}{\bar{z}_i - z_i^{**}}\right] + \rho \sum_{i=1}^{M} \frac{f_i(\mathbf{x})}{\bar{z}_i - z_i^{**}} \\ \text{subject to:} \quad & \mathbf{g(x)} = (g_1(\mathbf{x}), \ldots, g_m(\mathbf{x}))^T \leqslant 0, \end{aligned} \tag{3}$$

For objectives not belonging to $I^\leqslant$ class, $\bar{z}_i$ is set to z_i^*. The denominator of the terms in the objective function are different, thereby causing a different reference direction for the resulting AASF problem. Notice that no additional constraint is used in this formulation, thereby ignoring ε_i information. The resulting solution may not satisfy $f_i(\mathbf{x}) \leqslant f_i(\mathbf{x}^h)$ constraint for $i \in I^< \cup I^\leqslant \cup I^=$ and $f_i(\mathbf{x}) \leqslant \varepsilon_i$ for $i \in I^\geqslant$,

In the next sub-problem formulation, the scalarizing function used, comes from the reference point method [6]:

$$\begin{aligned} \underset{(\mathbf{x})}{\text{Minimize}} \quad & \max_{i=1,\ldots,M} \left[\frac{f_i(\mathbf{x}) - z_i^{**}}{z_i^{\text{nad}} - z_i^{**}}\right] + \rho \sum_{i=1}^{M} \frac{f_i(\mathbf{x})}{z_i^{\text{nad}} - z_i^{**}} \\ \text{subject to:} \quad & \mathbf{g(x)} = (g_1(\mathbf{x}), \ldots, g_m(\mathbf{x}))^T \leqslant 0, \end{aligned} \tag{4}$$

This formulation does not use $\bar{z}_i$ or ε_i information.

The scalarizing function used in the fourth sub-problem formulation to be introduced is related to the one used in the GUESS method [16]:

$$\begin{aligned} \underset{(\mathbf{x})}{\text{Minimize}} \quad & \max_{i=1,\ldots,M} \left[\frac{f_i(\mathbf{x}) - z_i^{\text{nad}}}{z_i^{\text{nad}} - \bar{z}_i}\right] + \rho \sum_{i=1}^{M} \frac{f_i(\mathbf{x})}{z_i^{\text{nad}} - \bar{z}_i} \\ \text{subject to:} \quad & \mathbf{g(x)} = (g_1(\mathbf{x}), \ldots, g_m(\mathbf{x}))^T \leqslant 0, \end{aligned} \tag{5}$$

For objectives not in the $I^\leqslant$ class, $\bar{z}_i$ is set to z_i^*.

On solving the scalarized MOO problems 2, 3, 4 and 5, the solutions obtained are referred to as alternate solutions. If a specific alternate solution is not desirable, a number of intermediate points can be examined between two alternate solutions on a line joining them. In the last step, the Pareto-optimality of the final solution is guaranteed by solving the following additional problem with slack variables γ_i:

$$\begin{aligned} \underset{(\mathbf{x},\boldsymbol{\gamma})}{\text{Maximize}} \quad & \sum_{i=1}^{M} \gamma_i, \\ \text{subject to:} \quad & f_i(\mathbf{x}) + \gamma_i \leqslant f_i(\mathbf{x}^h), \quad i \in I^<, \\ & \gamma_i \geqslant 0, \quad i \in I^<, \\ & \mathbf{g(x)} = (g_1(\mathbf{x}), \ldots, g_m(\mathbf{x}))^T \leqslant 0. \end{aligned} \tag{6}$$

If the solution to the above problem is equal to $(\mathbf{x}^h, \mathbf{0})$, then $\mathbf{x}^h$ is guaranteed to be Pareto-optimal and it is appointed as the final solution. Finally, the solution process stops once the aspiration level of DMs is obtained.

NIMBUS is a flexible method where the DMs can proceed in several ways by providing information about the aspiration level in each iteration of the algorithm. The overall NIMBUS algorithm is provided below in step-by-step format with a mention of steps in which iSOM can be employed for a better understanding:

1) Given the MOO problem (1), find ideal point ($\mathbf{z}^*$) and estimate nadir point ($\mathbf{z}^{\text{nad}}$) using the pay-off table or other methods [1], or from a representative set of EMO solutions. Set a utopian point $\mathbf{z}^{**} = \mathbf{z}^* - \boldsymbol{\epsilon}$ (usually, $\epsilon_i = 10^{-3}$).
2) Choose a feasible starting point $\mathbf{x}^0$ and calculate a Pareto-optimal solution $\mathbf{x}^1$ as a *start point*, employing MPB with $I^< = \{1, \ldots, M\}$. Set h = 1.
3) Divide the objective functions into *five classes* $I^<, I^\leqslant, I^=, I^\geqslant$, and $I^{<>}$ at the point $\mathbf{f}(\mathbf{x}^h)$ such that $I^\geqslant \cup I^{<>} \neq \varnothing$ and $I^< \cup I^\leqslant \neq \varnothing$. They ensure that an improvement in an objective must come from a deterioration on at least one other objective. If either of the unions is empty, go to Item 10. Obtain the *aspiration levels* $\bar{z}_i^h$ for $i \in I^\leqslant$ and the *upper bounds* ε_i^h for $i \in I^\geqslant$ from the DM. (iSOM-aided)
4) Find at most four alternate solutions $\hat{\mathbf{x}}^{h,k}$ by solving each of the k-th sub-problems defined in (2, 3, 4 and 5) by the MPB routine. If $\hat{\mathbf{x}}^{h,k} = \mathbf{x}^h$ for all k, ask the DM whether (s)he wants to try *another classification*. If yes, set $\mathbf{x}^{h+1} = \mathbf{x}^h$, $h = h + 1$, and go to Item 3 for finding new set of *alternate solutions*. If no further classification is desired, go to Item 10. If $\hat{\mathbf{x}}^{h,k} \neq \mathbf{x}^h$ for any k, $\hat{\mathbf{x}}^{h,k}$ is an alternate solution. Go to Item 5 with all alternate solutions. (iSOM-aided)
5) Present $\mathbf{f}(\mathbf{x}^h)$ and all $\mathbf{f}(\hat{\mathbf{x}}^{h,k})$ to the DM. If the DM does not like any of the alternate solutions and *prefers* $\mathbf{f}(\mathbf{x}^h)$, set $\mathbf{x}^{h+1} = \mathbf{x}^h$, $h = h + 1$, and to go Item 3 for a different classification process. Otherwise, if the DM likes a specific alternate solution $\hat{\mathbf{x}}^{h,\bar{k}}$ more than other solutions, go to Item 6. Otherwise (the DM likes more than one solution in the set ($\mathbf{x}^h, \hat{\mathbf{x}}^{h,k}$)), the DM chooses two most preferred solutions out of the set ($\mathbf{x}^h, \hat{\mathbf{x}}^{h,k}$). Let us say that the two chosen solutions are $\mathbf{x}^A$ and $\mathbf{x}^B$. Set $\mathbf{d}^h = \mathbf{x}^A - \mathbf{x}^B$ and go to Item 7. (iSOM-aided)
6) At this step, the DM wants to continue from $\mathbf{f}(\hat{\mathbf{x}}^{h,\bar{k}})$. If $I^< \neq \varnothing$, set $\mathbf{x}^{h+1} = \hat{\mathbf{x}}^{h,\bar{k}}$, $h = h+1$, and go to Item 3 for finding a new set of alternate solutions arising from $\hat{\mathbf{x}}^{h,\bar{k}}$. Otherwise ($I^< = \varnothing$), the Pareto-optimality of $\hat{\mathbf{x}}^{h,\bar{k}}$ must be checked by setting $I^< = \{1, \ldots, M\}$ and employing the MPB method to solve the resulting problem (6). Let the solution be $\hat{\mathbf{x}}^h$ and set $\mathbf{x}^{h+1} = \hat{\mathbf{x}}^h$. Set $h = h + 1$, and go to Item 3. (iSOM-aided)
7) Compute P different criterion vectors uniformly $\mathbf{f}(\mathbf{x}^A + t_j\mathbf{d}^h)$, where $t_j = \frac{j-1}{P-1}$, $j = 1, \ldots, P$.
8) Produce P *intermediate* Pareto-optimal solutions $\bar{\mathbf{x}}^h$ from the computed criterion vectors employing the MPB method (with $I^< = \{1, \ldots, M\}$). Store all alternate solutions and intermediate solutions in a database D.
9) Present P intermediate criterion vectors to the DM and let the DM choose the *most preferred one* among them. Denote the corresponding solution by $\mathbf{x}^{h+1}$. Set $h = h + 1$. If DM further wants to generate P intermediate solutions between the two intermediate solutions $\mathbf{x}^A$ and $\mathbf{x}^B$, then go to Item 7. If the DM wants to continue to better solutions, go to Item 3, otherwise, go to Item 10. (iSOM-aided)
10) Check the Pareto-optimality of $\mathbf{x}^h$ by solving the problem (6). Let the solution be $(\tilde{\mathbf{x}}, \tilde{\gamma})$. If $\tilde{\mathbf{x}} = \mathbf{x}^h$, the final solution is $\tilde{\mathbf{x}}$, otherwise, go to Item 3, by setting $\mathbf{x}^h = \tilde{\mathbf{x}}$.

If the solution of the problem (6) is equal to $(\mathbf{x}^h, \mathbf{0})$, then $\mathbf{x}^h$ is guaranteed to be Pareto optimal and it can be appointed as final solution. If $\mathbf{x}^h$ is not Pareto-optimal, then $\hat{\mathbf{x}}$ is Pareto-optimal solution.

Note that the DM can be aided with an easy-to-use visualization method in arriving at a decision at all italicized tasks in Items 2, 3, 4, 7, and 9 to (i) Define Start point, (ii) provide a classification of objectives, and set aspiration and upper bounds, (iii) seek different alternate solutions if needed, (iv) generate intermediate solutions and (v) choose the most preferred out of P intermediate solutions or from database D. NIMBUS employs a few standard visualization techniques for DM to facilitate decision-making: (i) Bar chart technique (ii) Petal diagram technique, and (iii) Value path (or parallel coordinate plot (PCP)) technique. The applicability of bar chart and petal diagrams are limited only to a few solutions. For handling a large number of alternate solutions and intermediate solutions, it is often difficult to visualize and compare each solution with these methods. With value path visualization, although one can visualize a large number of solutions, it is difficult to get a clear idea of the trade-off information or infer disjoint, holes, closeness to constraint boundaries, nearness to other chosen solutions, or other features of the solutions, which would be crucial in making the above decisions. In this study, we propose the use of iSOM (described in the next section) to visualize NIMBUS solutions, such as the start point, alternate solutions, intermediate solutions, and, of course, the final solution. In addition, iSOM also permits visualizing NIMBUS solutions near the boundary of the Pareto-optimal front, near disjointed regions or holes, near-constraint solutions, and, importantly, the current location of the solutions in the front along with a clear idea of the extent of the unexplored and explored parts of the Pareto-optimal front for a continuation of the NIMBUS method. We shall demonstrate the use of iSOM in NIMBUS method through several examples in Sections V to VII.

III. Brief Introduction to Interpretable Self organizing Map (iSOM)

Self-organizing maps (SOM) is a type of Artificial Neural Network (ANN) that is based on unsupervised learning. It takes high dimensional data (each with n variables and one response) $\mathbf{v}$ = [$\mathbf{x}_1$,$\mathbf{x}_2$,…,$\mathbf{x}_n$,$\mathbf{y}$] as input and maps it into a low-dimensional space, generally, a two-dimensional representation of the input data. This two-dimensional representation consists of nodes, which are connected in a rectangular or a hexagonal grid to form a 'Map'. Each node (say j^{th}) is associated with the weight vector w_j = [m_1^j, m_2^j, …, m_n^j,

m_y^j] such that the dimension of weight vector is equal to dimension of data set. Training of SOM includes finding out the Best Matching Units (BMUs) and a weight update rule. It also preserves the topology of the high-dimensional input space into the low-dimensional space.

A. *Conventional Self Organizing Map (cSOM)*

Training in a conventional SOM (cSOM) algorithm consists of choosing a winner node called the Best Matching Unit (BMU). The BMU is a node that has the least distance from the selected data point in the n-dimensional input space. Upon identifying the BMU, the weight vector of the respective node and nodes in its neighborhood are modified based on the weight update rule. Details associated with BMU calculation and weight update rule for cSOM is discussed in [33]. In cSOM, both tasks of identifying the BMU and weight update consider the input as well as the response. As a consequence, cSOM is prone to self-intersection and folding, affecting visualization. Description about cSOM is provided in supplementary document. The reader is referred to [33] for additional details about cSOM. To overcome these issues, interpretable Self Organizing Map (iSOM) was introduced [34].

B. *Interpretable Self Organizing Map (iSOM)*

Thole et al [34] suggested a different BMU finding and weight update rule to avoid the folding and self-intersection of cSOM. Topology preservation and avoidance of the self-intersection are two key features that make iSOM better than cSOM. In iSOM, the BMU is calculated by using the input vector only, whereas the weight update rule during training considers the response only. Description about iSOM is provided in supplementary document. The reader is referred to [34] for additional details about iSOM. Details of the BMU calculation and weight update rule for iSOM is discussed in [34]. A recent study [26] has compared cSOM and iSOM in the context of visualizing multi-criterion Pareto-optimal solutions and demonstrated the advantage of iSOM clearly on several standard and real-world problems. We are now ready to discuss how the iSOM visualization method can be applied to make the NIMBUS application easier and more convenient for DMs.

IV. Proposed iSOM-based Visualization within NIMBUS Method

Nagar et al. [26] proposed the use of iSOM to visualize the Pareto-optimal front. In the current work, we extend iSOM's capabilities for convenient visualization of NIMBUS solutions, as discussed below. NIMBUS finds different solutions in different steps during the iterative process. Hence it is essential to distinguish those solutions and select the preferred solution based on their properties and relative positions in the Pareto optimal front. The following subsections address the different NIMBUS solutions, their relative position in Pareto optimal front and provides an unique color code scheme to iSOM nodes.

A. *Identifying Boundary Points of Pareto Disjoint Regions*

The boundary points of the Pareto disjoint region are identified from the unified distance matrix (U-matrix) of objective functions' iSOM component planes. U-matrix is a 2-D map that plots the distance between two neighboring nodes/cells in an intermediate node, [33]. Larger values of the intermediate nodes in U-matrix represent the disjoint region in Pareto optimal front. The objective function component planes' nodes/cells corresponding to larger value in U-matrix is identified and plotted using color code defined in Table I.(S.No. 1)

B. *Identifying Near-Constraint Points*

In order to visualize the near constraint violation Pareto-optimal solutions, the average of the normalized constraint violation value $G(\mathbf{x})$ is trained and plotted on a separate component plane G using iSOM. The values for generating the component plane G can be computed as follows:

$$G(\mathbf{x}) = \frac{1}{J}\sum_{j=1}^{J} \hat{g}_j(\mathbf{x})\left[\mathbb{1}(\hat{g}_j(\mathbf{x}) \leqslant 0)\right], \tag{7}$$

where, $\hat{g}_j(\mathbf{x})$ is the j-th normalized constraint [4] of $g_j(\mathbf{x}) - b_j \leqslant 0$ (b_j being the resource value) obtained as $\hat{g}_j(\mathbf{x}) = g_j(\mathbf{x})/b_j - 1 \leqslant 0$, J is the number of constraints, $\mathbb{1}$ is indicator function which takes value 1, if the Pareto-optimal solution $\mathbf{x}$ does not violate the j-th constraint, and 0, otherwise. Let us say that the number of feasible solutions are $n_f = |G(\mathbf{x})|$. In order to indicate the near-constraint points, we identify top 10% ($n_G = \lceil 0.1 \times n_f \rceil$) feasible solutions ($\mathbf{x}_G^k$, for $k = 1, \ldots, n_G$) close to the constraint boundaries by first sorting the points in descending order of G and picking the top 10% of points from the sorted list.

Then, respective cells ($\mathbf{c}_G^k$, for $k = 1, \ldots, n_G$) are found by finding the closest cell in the G component plane to each of the $\mathbf{x}_G^k$ solutions. These cells are plotted on each component plane using the color code defined in Table I (S.No. 2 and 3).

TABLE I
COLOR CODE FOR VISUALIZATION USING ISOM FOR DISTINGUISHING THE DIFFERENT NIMBUS SOLUTIONS AND SELECTING THE PREFERRED SOLUTION BASED ON THEIR PROPERTIES AND RELATIVE POSITIONS IN PARETO OPTIMAL FRONT. : EDGE (EDGE OF ISOM NODE), FACE (FACE OF ISOM NODE), COLOR (EDGE COLOR/ FACE COLOR OF CORRESPONDING ISOM NODE), NODE (FOR DEMO PURPOSE)

S.No.	Points	Edge	Face	Color	Node
1	Boundary points	Yes	No	Black	⬡
2	Near-constraint points	No	Yes	Grey	⬢
3	Start point/ current solution	No	Yes	Black	⬢
4	Selected points after classification	Yes	No	White	⬡
5	Un-selected points in respective objectives after classification	Yes	No	Red	⬡
6	Alternative solutions	No	Yes	Magenta	⬢
7	Intermediate solutions	No	Yes	Green	⬢
8	Final solution	No	Yes	Red	⬢

C. Selected Search Space after Classification

Every classification made in Task 3 of the NIMBUS method can provide the DMs an idea of selected and un-selected parts of the search space that can be visualized on iSOM component plane of objectives. For the current solution $\mathbf{x}^h$, all Pareto-optimal points which conform to the classification of objectives, provided by the DMs, can be identified and marked on the respective iSOM component plane of objectives. They represent the selected Pareto points for the current iteration. Such a visual check can allow the DMs to make a final consideration in leaving Item 3. In addition, the cells that do not conform to the provided classification of objectives can be marked in a different color and style to indicate the opposite. The respective color code scheme for both selected and un-selected search regions are shown in Table I (S.No. 4 and 5).

D. NIMBUS Points

Every iteration of the NIMBUS method begins with several key points: (i) current point ($\mathbf{x}^h$) (or, a user-specified start-point $\mathbf{x}^0$) in Item 2, (ii) a derived MPB solution $\hat{\mathbf{x}}^h$ in Item 4, and (iii) several created intermediate points $\bar{\mathbf{x}}^h$ in Item 7, of which the most preferred solution is chosen in Item 9. In addition to visualizing these solutions using iSOM component planes for a better understanding of the NIMBUS method, another important solution to include in the visualization process is the final point ($\tilde{\mathbf{x}}$) of the overall NIMBUS method. The respective iSOM cells can be marked differently for each of the above points (described in Table I -S.No. 6 to 8) to have a better comprehension of the progress of NIMBUS method.

E. Augmentation of NIMBUS with Focused EMO Algorithm

In the event of fewer points in the vicinity of intermediate solutions in Item 8, a focused EMO algorithm, such as R-NSGA-II [35] or R-NSGA-III [36] or other methods can be employed. These methods use a population-based evolutionary multi-objective optimization method to find multiple trade-off solutions in a focused region on the Pareto-optimal front dictated by a DM-supplied reference point $\mathbf{z}^r$ and a shrinkage factor (μ). In this study, we choose them as follows:

$$\mathbf{z}^r = \frac{\mathbf{F}^{alt1} + \mathbf{F}^{alt2}}{2}, \tag{8}$$

$$\mu = \max_{i=1}^{M} \left[\frac{|f_i^{alt1} - f_i^{alt2}|}{f_i^{\max} - f_i^{\min}} \right], \tag{9}$$

where $\mathbf{F}^{alt1}$ and $\mathbf{F}^{alt2}$ are two alternate MPB solutions and $f_i^{\min}$ and $f_i^{\max}$ are the minimum and maximum values of i-th objective function. Focused EMO approaches create a set of well-distributed reference points on a unit simplex close to $\mathbf{z}^r$ and then shrink the points by μ to make them closer to each other. Thereafter, a reference point-based EMO procedure, such as NSGA-III [6], is applied to find respective focused Pareto-optimal points close to the alternate solutions. After generating the focused solutions, DM can plot them in iSOMs on the objective function space and visualize the preferred solution only, instead of on the complete Pareto-optimal front. The visualization of NIMBUS solution on the component plane of preferred solutions allows the larger spread as compared to the component plane of the complete Pareto optimal solution. Thus, visualization of NIMBUS solutions on the component plane of preferred solutions can also be referred to as *local visualization using EMO*.

F. Proposed iSOM-aided NIMBUS method

The steps of iSOM aided NIMBUS are discussed below:

Step 1: Obtain a set of complete Pareto optimal front for the given MOO using an EMO procedure.

Step 2: Plot iSOM component plane for each objective and constraint function using Pareto-optimal points after Item 1 of the NIMBUS method.

Step 3: Identify the Pareto disjoint regions using U-matrix and plot them on iSOM component planes as per the color code defined in Table I.

Step 4: Plot near-constraint points on the component plane of objective functions and the average of normalized constraint violation component plane G.

Step 5: Select the start point or current point on iSOM component planes. (Item 2 in NIMBUS algorithm)

Step 6: At the start point or current point, define the NIMBUS classification according to the desired aspiration/upper level and visualize selected and un-selected Pareto regions on the iSOM component planes of objectives. (Item 3 in NIMBUS algorithm)

Step 7: Obtain and plot alternate solutions on iSOM component plane. (Item 4 in NIMBUS algorithm)

Step 8: If DM wants to further classify the objective functions at an alternate solution, go to Step 6, otherwise select two alternate solutions aided by iSOM visualization. (Items 5 and 6 in NIMBUS algorithm)

Step 9: Generate intermediate solutions between two alternate solutions (if DM wants to explore more points) and plot it using iSOM, go to Step 11. (Item 7 in NIMBUS algorithm)

Step 10: If DM wants to visualize solutions locally, generate focused EMO solutions by R-EMO algorithm using Equations 8 and 9 and visualize locally.

Step 11: If aspiration level is attained, select the final solution and mark it on the iSOM component plane; otherwise go to Step 8. (Items 9 and 10 in NIMBUS algorithm)

A flowchart of the main steps is provided in the supplementary document.

V. Results of iSOM-NIMBUS Procedure on Crash-worthiness Problem and Its Advantages

In this section, the proposed methodology to visualize the NIMBUS solutions using the iSOM approach is discussed in detail on the crash-worthiness problem [36]. Crash-worthiness problem is an unconstrained MOO problem with three objective functions and five design variables. The decisions in various stages of the NIMBUS method adopted here are purely based on the author's choice. They allowed to demonstrate how the iSOM-aided NIMBUS procedure can be used conveniently. Any other decision by DMs can also be implemented similarly.

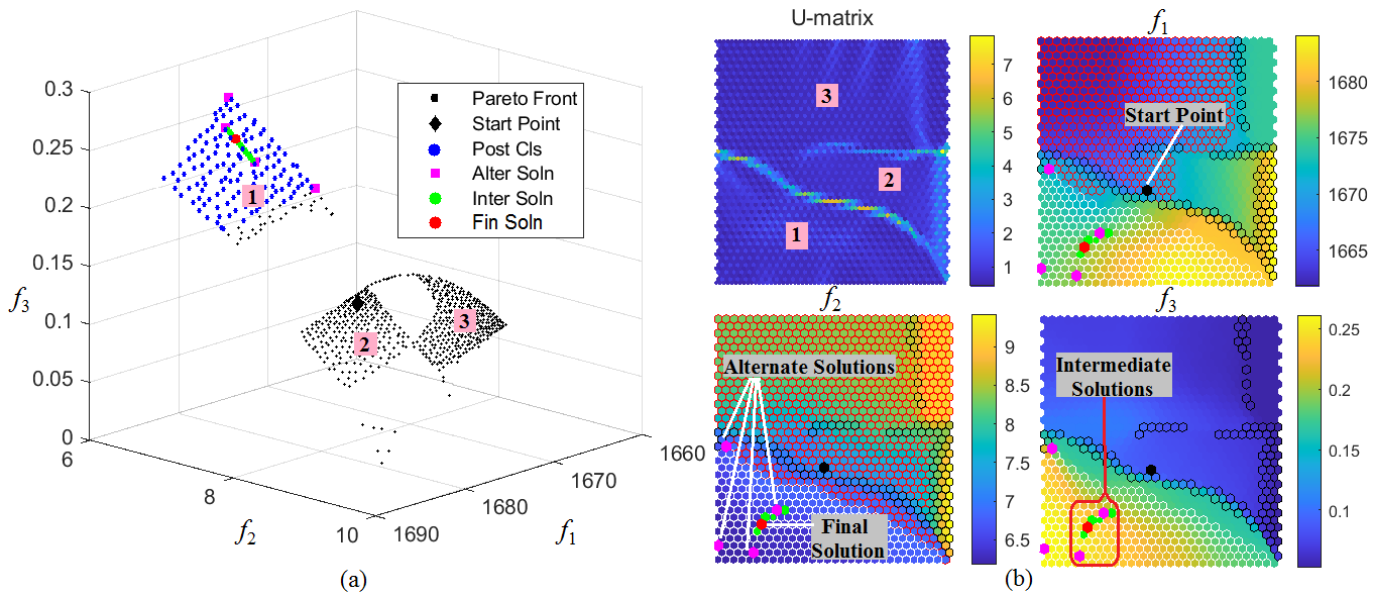


Fig. 1. Crash worthiness problem: (a) Scatter Plot of NSGA-III-obtained Pareto solutions are marked with NIMBUS solutions, blue markers depict search space selected after classification, (b) U-matrix plot indicates Pareto boundary cells having relatively large values of U, indicating three clear clusters that exist on the obtained Pareto front. f_1, f_2 and f_3 are component plane of objective functions, for which each cell indicates the respective f_i values. Cells with black edge color depict Pareto disjoint boundary inferred from the U-matrix. The cells with red and white edge colors represent objective-wise un-selected points and selected points respectively after classification. The cells with black face color represent the start point, magenta face color represent alternate solutions, green face color represents intermediate solutions, and red face color represents the final solution. The color code scheme is provided in Table I.

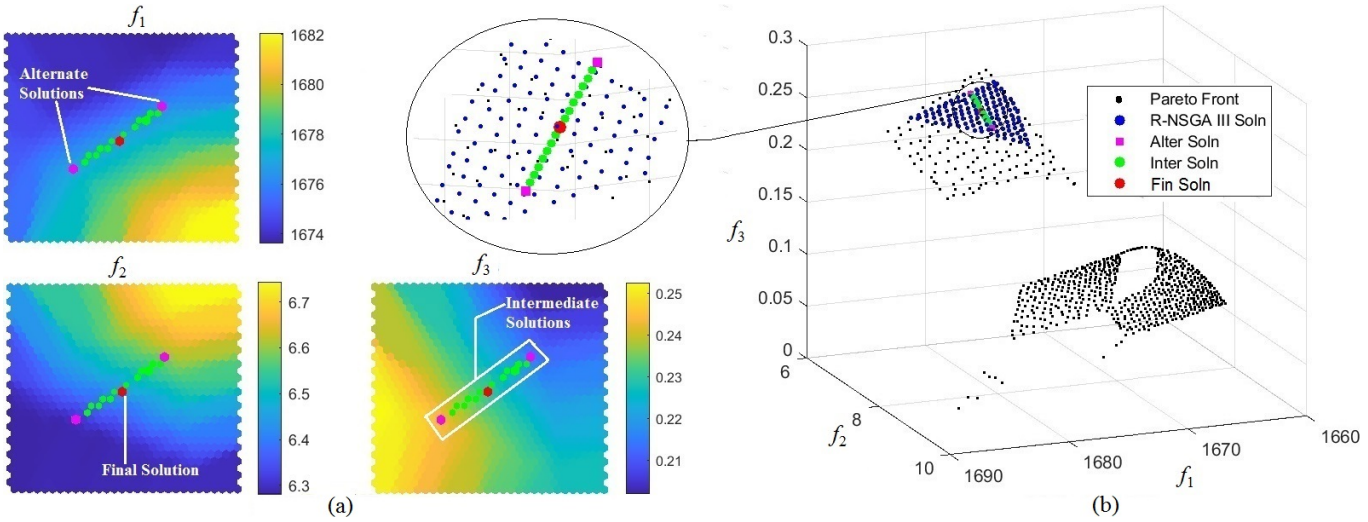


Fig. 2. Crash-worthiness problem: (a) iSOM component plane of objectives, (b) Scatter plot of R-NSGA-III points in the context of the entire Pareto-optimal front. The region of interest is blown up for clarity. The use of focused R-NSGA-III iSOM component planes allows a more convenient decision-making approach.

A. *Using Complete Pareto-optimal Front*

A scatter plot of a representative set of Pareto-optimal solutions in the entire search domain obtained using the NSGA-III procedure [6] is shown in the Fig. 1(a) in small dots as Step 1. In Step 2 the iSOM procedure is applied to the Pareto data set to obtain the component planes of each objective function. To facilitate our discussions, the objective vectors of the set are checked for clusters using the U-matrix in iSOM. U-matrix plot shows the existence of three different clusters in the entire Pareto set. The three clusters are seen and marked in the scatter plot in Step 3. Ideal, utopian, and nadir points are estimated from the complete set for NIMBUS computations. The start point of the NIMBUS method is chosen to be around the centroid of the Pareto set and is marked with a black-colored diamond. This point falls in cluster 2. This completes Step 5. Lets say the DM chooses the start solution as: $\mathbf{x}^0 = (x_1, x_2, x_3, x_4, x_5) = (2, 2, 2, 2, 2)$ with start criterion vector $\mathbf{z}^0 = (f_1, f_2, f_3) = (1683.130, 9.630, 0.120)$, resulting in $\mathbf{z}^1 = (1668.870, 7.130, 0.090)$ on the Pareto-optimal front is shown in black face color in three iSOM component planes of the objectives. At the start point, a classification of objective functions is first defined by the DM as-

$$I^{<} = \varnothing, I^{\leqslant} = \{2\}, I^{\geqslant} = \{1\}, I^{=} = \varnothing, I^{<>} = \{3\},$$

with an aspiration level of $\bar{z}_2 = 6.85$ and $\varepsilon_1 = 1680$. This implies that DM wishes to improve on f_2 at the expense of increasing f_1 while letting f_3 change freely. However, approximate values for aspiration level $\bar{z}_i$ and upper bound ε_i can be chosen, if it is not known explicitly to the DM.

The un-selected cells after classification are shown by red edge color in the respective iSOM component planes of objectives. As objective f_3 can change freely, there is no un-selected points after classification. Hence, f_3 iSOM component plane has no cells with red edge color. The selected cells after classification are highlighted by white edge color in iSOM component plane of each objective. It is clear from the iSOM component planes that classification $I^{\leqslant} = \{2\}$ overrides $I^{\geqslant} = \{1\}$, as red edge color zone in f_2 iSOM component plane contains the red edge color zone in f_1 iSOM component planes. This completes Step 6. In Step 7, the resulting four MPB solution is obtained based on the above classification. All the four MPB solutions with objective vectors $\mathbf{z}^{1,1} = (1671.421, 6.839, 0.188)$, $\mathbf{z}^{1,2} = (1675.490, 6.143, 0.264)$, $\mathbf{z}^{1,3} = (1676.166, 6.583, 0.217)$ and $\mathbf{z}^{1,4} = (1677.054, 6.295, 0.244)$ are different from the start-point $\mathbf{z}^1$, so they are declared as alternate solutions. It is clear that two of the four alternate solutions (magenta face color) lie on the edge of the Pareto front. Also, the iSOM component planes of objectives indicate that the two alternate solutions in the edges have extreme values of f_2 and f_3. In Step 5, if DM is not comfortable in choosing the edge points, DM is left with two intermediate alternate solutions $\mathbf{z}^{1,3}$ and $\mathbf{z}^{1,4}$, for which all three objectives seem to have a good compromise in them as Step 8. To create more points in the vicinity, the DM has an option of generating a maximum of $P = 15$ reference points in between them in Step 7. In Step 8, 15 different Pareto-optimal *intermediate* solutions are found solving ASF problem (Eqs.2, 3, 4 and 5) by classifying all objectives in $I^{<}$ class. Once again, the iSOM component planes of objectives reveal that the intermediate solution (green face color) near the middle of all 15 intermediate solutions makes a better trade-off (near-average objective values of 15 intermediate solutions) in all three objectives. Thus, in Step 9, the intermediate solution marked using a red-faced cell is chosen. Since it is a Pareto-optimal solution, the NIMBUS method is terminated with the red-faced cell solution as the final solution $\mathbf{z}^2 = (1676.777, 6.392, 0.235)$ of the iSOM-NIMBUS procedure as Step 11.

B. *Using a Focused Set of Pareto-optimal Solutions*

It can be seen from Fig. 1 that most of the NIMBUS decision-making activities took place at the bottom-left corner of the iSOM component planes. DM's classification choice can take such activity anywhere on the Pareto-optimal front. A more clear visualization can be achieved if the decision-making activity can be carried out at a focused part of the Pareto-optimal front dictated by the alternate solutions obtained in Step 5. In this section, we take the help of a reference point-based NSGA-III procedure [36] for this purpose. We discuss the procedure here.

First, instead of NSGA-III, R-NSGA-III solutions are found and stored to create iSOM component planes. Reference point and shrinkage factor are calculated based on Equations 8 and 9 using the two chosen alternate solutions:

$$\begin{aligned}\mathbf{z}^r &= \frac{(1676.166, 6.583, 0.216) + (1677.054, 6.295, 0.244)}{2},\\ &= (1676.610, 6.439, 0.230),\\ \mu &= \max\left[\frac{0.888}{33.492}, \frac{0.288}{4.603}, \frac{0.028}{0.225}\right],\\ &= \max\left[0.026, 0.063, 0.124\right] \;=\; 0.124.\end{aligned}$$

Next, iSOM component plane plots of objectives are made using R-NSGA-III solutions, and all 15 intermediate solutions including the two alternate solutions are marked in Fig. 2. For relevance, the R-NSGA-III solutions are also shown in the original scatter plot (Fig. 2(b)). It can be seen that 15 intermediate solutions are now more visible. The trade-off in objective values for 15 solutions is also clear, allowing the DM to make a choice in choosing the final solution ($\mathbf{z}^2$) with more confidence. The final choice is a solution that lies in the middle of the two alternate solutions for which all three objectives take an average value, making it a good trade-off solution among all 15 solutions. The color-contoured iSOM component plane plots of objective allow a DM to investigate the sensitivity of objectives in moving from one intermediate solution to the next and make a decision. This completes Step 10 of the iSOM aided NIMBUS procedure.

C. *Contrasting with NIMBUS visualization techniques*

NIMBUS method includes several inbuilt visualization techniques. The parallel coordinate plot (PCP) (or the value path plot) is one of the best visualization techniques available in NIMBUS. In order to demonstrate the complete NIMBUS procedure on a PCP, we first show all NSGA-III-obtained Pareto-optimal solutions (Step 1 of NIMBUS procedure) in Fig. 3 with green lines for the crash-worthiness problem. We add a fourth vertical axis (in addition to three objective axes) to show the addition of NIMBUS points in different stages. The inclusion of NSGA-III solutions is the first stage of the PCP. In stage 2, the start-point (Step 2 of NIMBUS procedure) is shown with a white line. Four alternate solutions were found in Step 4 of NIMBUS procedure with yellow lines. The PCP clearly shows that all four solutions are associated with a small f_2 value and a relatively high f_3 value. By looking at the PCP, it is difficult to conclude that two of the four alternate solutions lie on the edge of the Pareto-optimal front. Only one of the four solutions has the largest f_3 value and smallest f_2 value. While this solution can be considered to lie on the edge, the second near-edge solution is difficult to comprehend. In comparison, iSOM component plane of objectives in Fig. 1 clearly shows that two alternate solutions lie close to the edge of the Pareto front.

Next, in the stage 4, 15 intermediate solutions are shown with red lines. While they lie in between the two pivoting alternate solutions chosen to create them, some trade-off in objectives can be observed from the PCP. But the true trade-off among the solutions is not apparent. The final solution chosen using iSOM-NIMBUS procedure is marked in stage 5,

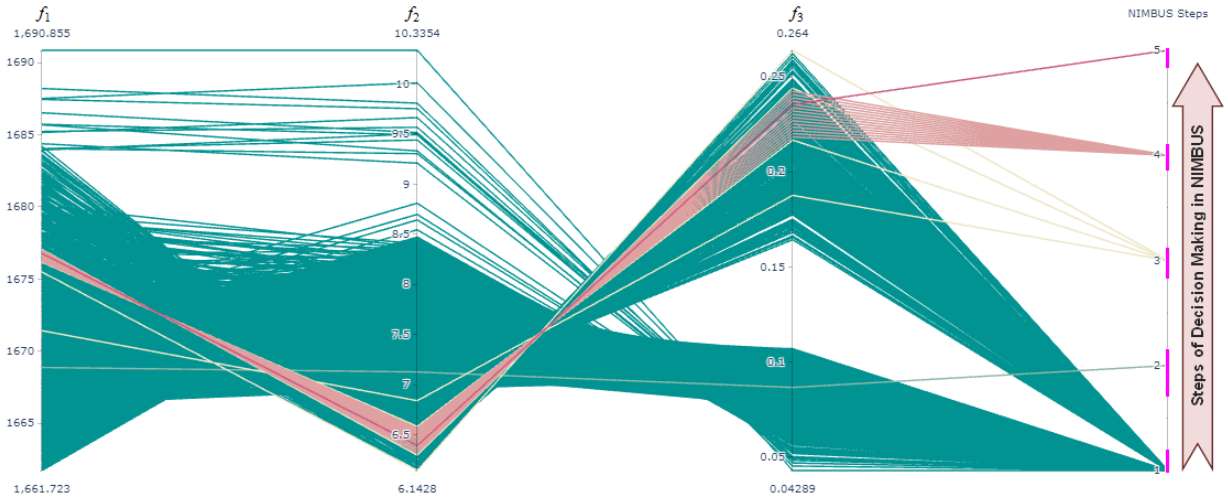


Fig. 3. PCP on crash-worthiness problem: f_1,f_2 are f_3 are objective function axes, whereas NIMBUS Steps: 1 represents Pareto front, 2 represents start point, 3 represents alternate solutions, 4 represents intermediate solutions and 5 represents the final solution.

but if an average trade-off solution would have been the choice, a different solution passing through the middle of two pivoting alternate solutions in each objective axes should have been chosen. Clearly, the PCP does not provide a true idea of the location of a point in the perspective of the entire Pareto-optimal front. PCP does not also provide true trade-off information. It certainly cannot show clusters, holes, and discontinuity in the Pareto-optimal front. Hence, reliable visualization-based decision-making becomes a difficult task using PCP. They can be used to passively demonstrate a set of trade-off solutions, as a trade-off in objectives occurs only if there is criss-crossing of lines in two neighboring objective axes in a PCP.

VI. Results on Benchmark Problems

A. *The five-objective Problem from NIMBUS Study*

Naru-weiss problem is a two-variable, five-objective unconstrained multi-objective optimization problem [37]. The formulation for this problem is given in the supplementary document. In Fig. 4(a), three objectives f_1, f_2 and f_3 are represented on three axes. f_4 is represented by the marker size (proportional to its value) and f_5 is represented by the color (blue to yellow indicating low to high value).

From Fig. 4(a), it is clear that the objective functions f_1 and f_3 are conflicting in nature. Also, f_2 and f_4 are in conflict to each other. The objective function f_5 has a small value at one certain location (dark blue region) and then increases rapidly outwards from that location. The same inference can be drawn from the component plane of objective functions depicted in Fig. 4(b).

From the start point (dark black cell indicating minimum of f_5), DM provides the following classification of objectives:

$$I^{<} = \{1,2\}, I^{\leqslant} = \varnothing, I^{\geqslant} = \{3,4\}, I^{=} = \varnothing, I^{<>} = \{5\},$$

with $(\varepsilon_3, \varepsilon_4)$ = (-4.5,0.45) (worsening f_3 and f_4 till some limit), letting f_5 change freely and hoping to improve f_1 and f_2 as much as possible. Four sub-problem formulations find four independent alternate solutions, marked with magenta cells. One alternate solution at the edge of Pareto front is discarded. Then, randomly two out of three alternate solutions are selected and 15 intermediate solutions are computed in between them using the procedure described in Step 9 of the iSOM aided NIMBUS procedure, of which one solution (red face cell) is chosen as the final solution (see Table I for a summary of iterative solutions for this and other problems of this paper in the supplementary document). The start point, alternative and intermediate solutions, and the final solution are marked in Fig. 4, using the color code defined in Table I.

If we observe the iSOM component planes of objectives, we can conclude that the start point corresponds to small values of f_3, f_4, and f_5, whereas moderate values of f_1 and higher values of f_2 can also be verified from the scatter plot in Fig. 4(a) as well. Out of two alternate solutions, one alternate solution corresponds to a large value of f_2, f_3 and f_5 component planes, whereas small values of f_1 and f_4 planes that can be verified from scatter plot in Fig. 4(a) as well. It is evident from Fig. 4(b) that the intermediate solutions spread in large values of f_5 component plane, but having small values of f_1 and f_4 component planes and spanning across large to small values in f_2 and f_3 component planes. The final solution (shown as a red face cell) makes a good compromise in values of all five objectives among 15 intermediate solutions. Besides making a good compromise, the final solution is also away from the Pareto boundary and well inside the feasible space. Without the iSOM component plane plots of the objectives, such decision-making would have been difficult to achieve. The final solution is sent to Item 10 of NIMBUS algorithm for a final Pareto-optimality check before termination of the overall NIMBUS-iSOM procedure. The iSOM component planes of objectives also allow DM to have clear ideas of (i) centrality (or boundary) of the solutions in the Pareto-optimal front, (ii) proximity to constraint boundaries, and (iii) a trade-off among objectives. The methodologies described in the PaletteViz study [38], [39] in identifying *knee* point, a hole, and other peculiarities can be considered and marked appropriately on the iSOM component planes for additional

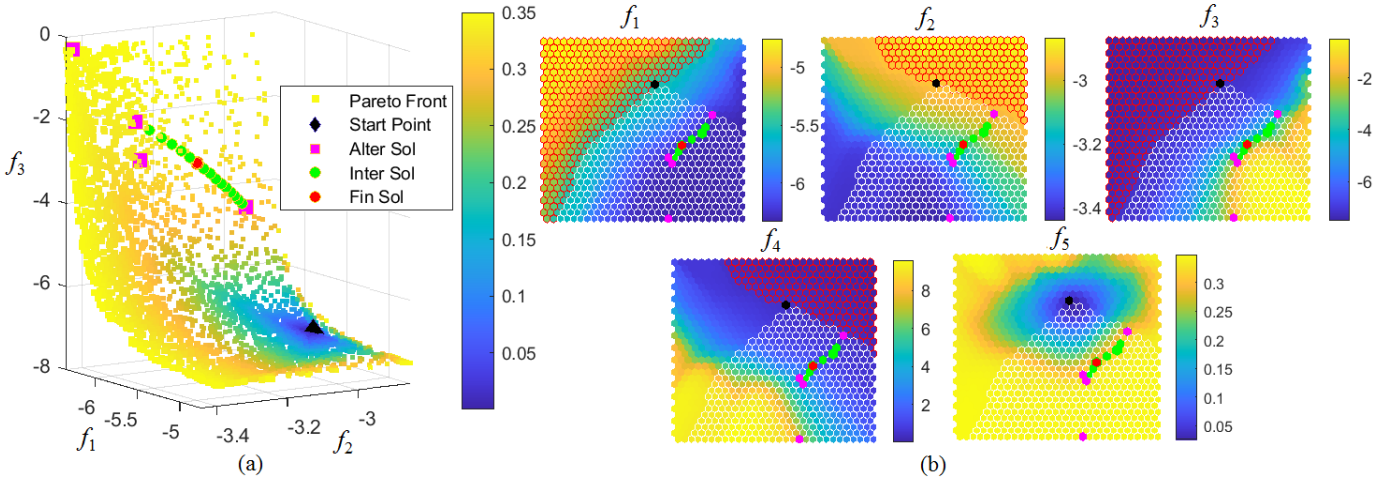


Fig. 4. Naru weiss problem (a) 5-d Scatter plot obtained from NSGA-III Pareto optimal points, f_1,f_2 and f_3 on axes, f_4 is represented by marker size and f_5 is represented by the color bar, Selected part of search space after classifications are shown by blue markers, (b) iSOM component planes of objective functions f_1,f_2,f_3,f_4 and f_5. Un-selected points and selected points in search space after classification and all the NIMBUS critical points have been represented by cells with the color code scheme provided in Table I.

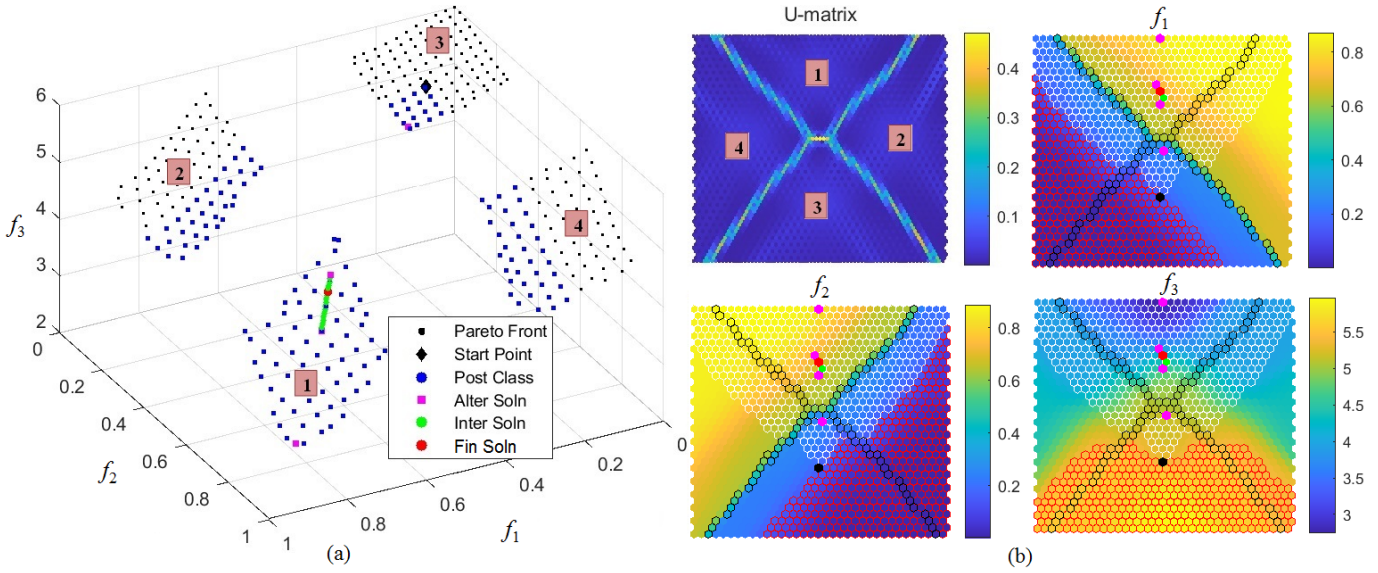


Fig. 5. DTLZ7 problem: (a) NSGA-III-obtained Pareto points and the NIMBUS solutions. Selected part of search space after classification are shown by blue markers. (b) iSOM component planes of objectives, selected and un-selected points after classification and all critical NIMBUS points.

aid in decision-making.

B. A Disjointed Pareto Set Problem: DTLZ7

DTLZ7 problem has three objective functions and the Pareto optimal front is separated by four disjoint regions [40]. The scatter plot of the Pareto-optimal front obtained using NSGA-III and their classification, obtained using the U-matrix of the iSOM component planes, into four clusters are shown in Fig. 5(a). The start point is shown with a blue diamond, which happens to fall on cluster 3. The following classification is made by the DM:

$$I^{<} = \varnothing, I^{\leq} = \{3\}, I^{\geq} = \{1,2\}, I^{=} = \varnothing, I^{<>} = \varnothing,$$

with $\bar{z}_3 = 5.25$ (improving f_3 with a limit) and $(\varepsilon_1, \varepsilon_2) = (0.859, 0.859)$ values (at the expense of worsening f_1 and f_2 within limits). The selected points after classification are shown with blue marker color in the figure.

The respective iSOM component planes of objectives are shown in Fig. 5(b). It is clear that the start point falls on cluster 3 and is somewhat away from the Pareto boundary. Step 7 finds four alternate solutions, marked with magenta face color. These points are marked on the iSOM component planes of objectives. Clearly, despite the start point's location in cluster 3, the alternate solutions obtained by solving four sub-problems produce three points on cluster 1 and one in cluster 3. These points are also marked in the scatter plot in Fig. 5(a) for clarity, but a good idea of the location of all four alternate points is clear from iSOM component plane plots of the objectives. At Step 8, two preferred alternate solutions – two interior points having a good trade-off among all three objectives – are chosen by the DM. In Step 9,

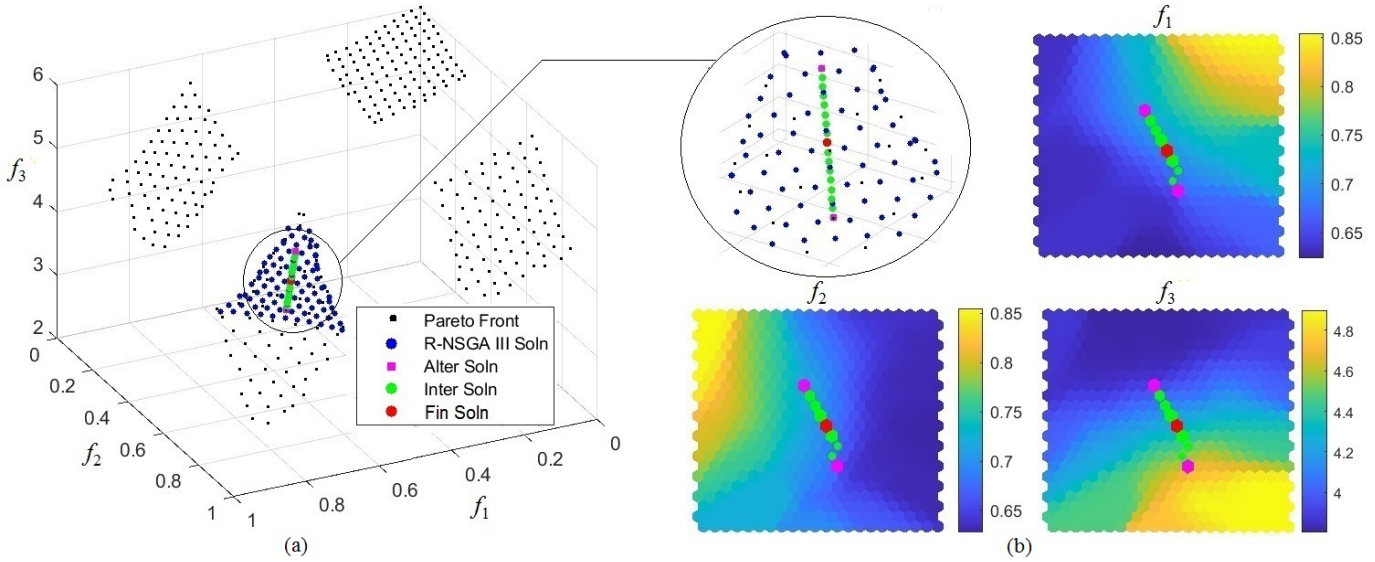


Fig. 6. DTLZ7 problem: (a) R-NSGA-III-obtained Pareto points and the NIMBUS solutions.(b) iSOM component planes of objectives using focused Pareto points and all critical NIMBUS points.

15 intermediate solutions (marked in green cells) are found systematically within the two preferred alternate solutions. Finally, a solution from the center region of all intermediate solutions is chosen as the final solution (shown with a red cell). A final Pareto-optimality check of the final solution will terminate the decision-making process.

In this problem, the two chosen alternate solutions and the resulting 15 intermediate solutions lie in one of the four clusters (cluster 1). To have a more clear visualization and decision-making, R-NSGA-III can be employed to obtain a set of focused Pareto-optimal points to develop iSOM component plane plots of the objectives using the reference point $\mathbf{z}^r = (0.7863, 0.7863, 3.2591)$ and shrinkage factor $\mu = 0.2$. Fig. 6(a) replots the scatter plot with R-NSGA-III points. Fig. 6(b) show iSOM component planes of objectives using R-NSGA-III points only. The two preferred alternate solutions and 15 intermediate points are also marked on the iSOM component planes of objectives. The final solution can now be seen to lie at a good compromise region of each objective and almost at the center of the R-NSGA-III obtained Pareto-optimal region. Whenever more focused decision-making needs to be performed to better visualize the trade-off in objectives, the original NSGA-III can be replaced with R-NSGA-III to find a focused set of points for clarity and more convenient decision-making.

C. *Constrained Problem: C2-DTLZ2*

Next, we consider a constrained test problem: three-objective C2-DTLZ2 problems. NSGA-III points are shown in Fig. 7(a). Decision-making in the presence of constraints requires a clear visualization framework revealing near constraint solutions. This problem is chosen to demonstrate the effectiveness of iSOM visualization method for this purpose.

The iSOM U-matrix plot reveals that there are four clusters in the Pareto-optimal front and also identifies the boundary points of each cluster. The boundary points, marked with grey markers, happen to fall on the constraint boundary. The start point is found to be at the center of the complete Pareto-optimal front, marked with a black diamond. The iSOM component planes shown in Fig. 7(b) also mark the start point. The boundary of each cluster is also clearly shown in iSOM component plane plots of the objectives. Following classification rules are provided for this problem:

$$I^{<} = \varnothing, I^{\leqslant} = \{1, 3\}, I^{\geqslant} = \varnothing, I^{=} = \varnothing, I^{<>} = \{2\},$$

with $(\bar{z}_1, \bar{z}_3) = (0.3, 0.5)$ (improve f_1 and f_3 to their limits) at the expense of possible worsening of f_2 without any limit. Notice that four sub-problems in Item 3 of NIMBUS algorithm produce three alternate solutions, marked with magenta cells in iSOM component plane plots of the objectives. Of these three points, two falls on the constraint boundary and one at the extreme of cluster 2. The nearness of constraint boundary and extreme position on cluster 2 is clear from iSOM component planes as well. Each of the constraint boundary solutions is paired up with the extreme solutions and 15 intermediate solutions are found for each pair. It can be seen from iSOM component plane plots of the objectives that all 30 intermediate solutions correspond to small values of f_1, large values of f_2, and small to intermediate values of f_3. A good compromise solution lying close to the centroid of the intermediate solutions is chosen as the final solution (shown in red color).

A separate iSOM component plane plot for the constraint is shown for this problem. The near constraint cells, boundary points, and ensuing alternate and intermediate solutions are shown in the plot, allowing DM to choose a final solution that is away from the constraint boundary but also not too close to the extreme Pareto solution. This level of visualization and understanding of Pareto-optimal points on the entire Pareto front or a focused part of the Pareto front is rare in standard Pareto visualization methods. Despite requiring several iSOM component planes, they, together, allow a more convenient decision-making environment revealing critical functionalities

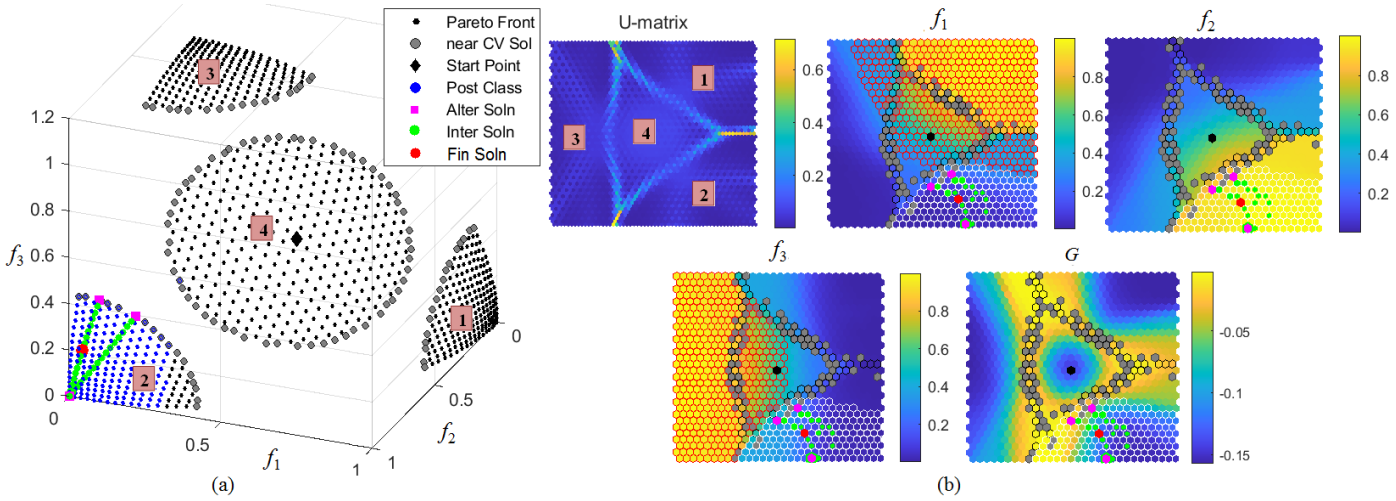


Fig. 7. C2DTLZ2 problem: (a) NSGA-III-obtained Pareto points, NIMBUS solutions and selected part of search space after classification. (b) iSOM component planes of objectives using complete Pareto points, selected and un-selected points after classification and all critical NIMBUS points.

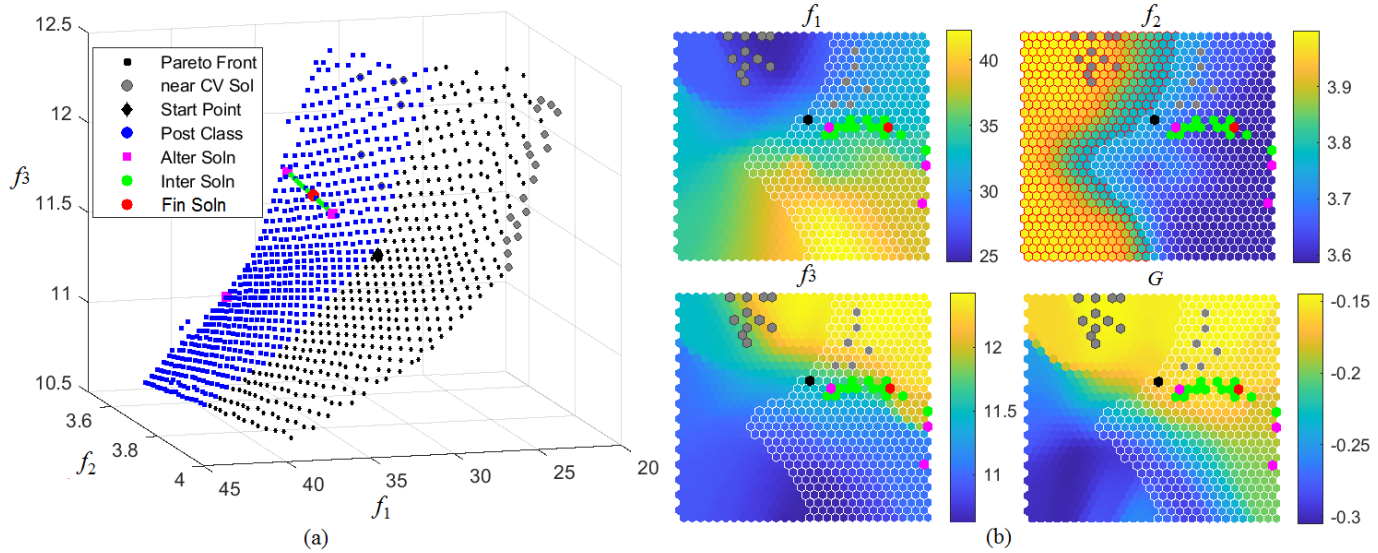


Fig. 8. Carside impact problem: (a) NSGA-III-obtained Pareto points and the NIMBUS solutions. Selected part of search space after classification. (b) iSOM component plane plots of the objectives using complete Pareto points, selected and un-selected points after classification and all critical NIMBUS points.

associated with a problem. This example demonstrates the sensitivity of the decision-making task in arriving at a final preferred solution and the importance of an easier and more revealing visualization framework for performing convenient and effective decision-making for multi- and many-objective optimization.

VII. Results on Real-world Problems

A. *Carside impact problem*

Carside impact problem is a three-objective, 10-constraint problem, in which the weight of the car, the pubic force experienced by a passenger, and the average velocity of the V-pillar responsible for withstanding the impact load need to be minimized [20]. This problem will allow us to demonstrate the iSOM-based visualization in the presence of constraint/s on a real-world problem.

NSGA-III points are shown in Fig. 8(a) for a reference since the objective space is three-dimensional. The resulting iSOM component planes (three objectives and constraint violation) are shown in Fig. 8(b). Note that a non-zero constraint violation $G(\mathbf{x})$ point (Eqn. 7) implies it is feasible. The start point on the Pareto front is shown with a black colored cell on all four iSOM component planes. At the start point ($\mathbf{z}^1 = (31.180, 3.756, 11.411)$), the DM makes the following classification:

$$I^{<} = \varnothing, I^{\leqslant} = \{2\}, I^{\geqslant} = \varnothing, I^{=} = \varnothing, I^{<>} = \{1, 3\}.$$

This means the DM wishes to improve f_2 with a limit $\bar{z}_2 = 3.75$ and allowing f_1 and f_3 to change freely. Fig. 8 (both a and b) shows the possible cells (or solutions) that satisfy the above classification and are selected for further search. The respective cells are marked with white-bordered cells and the un-selected cells are marked with red-bordered cells. Cells that are close to the constraint boundary are marked in grey color. Step 7 produces three distinct alternate solutions, marked in magenta color. Two alternate solutions

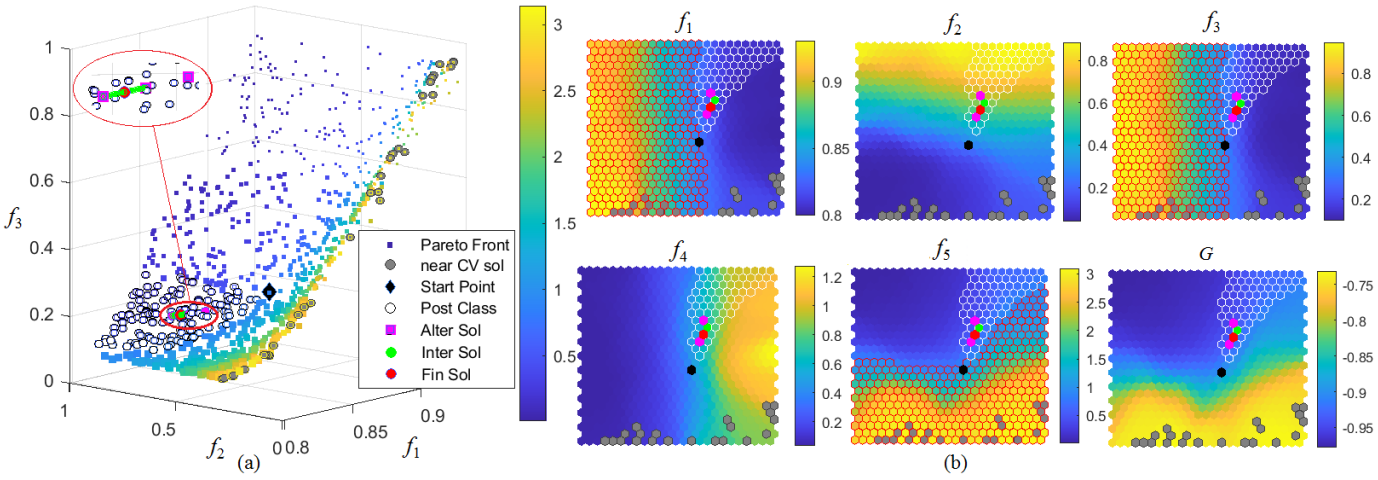


Fig. 9. WATER problem: (a) NSGA-III-obtained Pareto points, NIMBUS solutions and selected part of search space after classification. (b) iSOM component planes of objectives using complete Pareto points, selected and un-selected points after classification and all critical NIMBUS points. In iSOM component plane one alternate solution and the final solution have shared the same node.

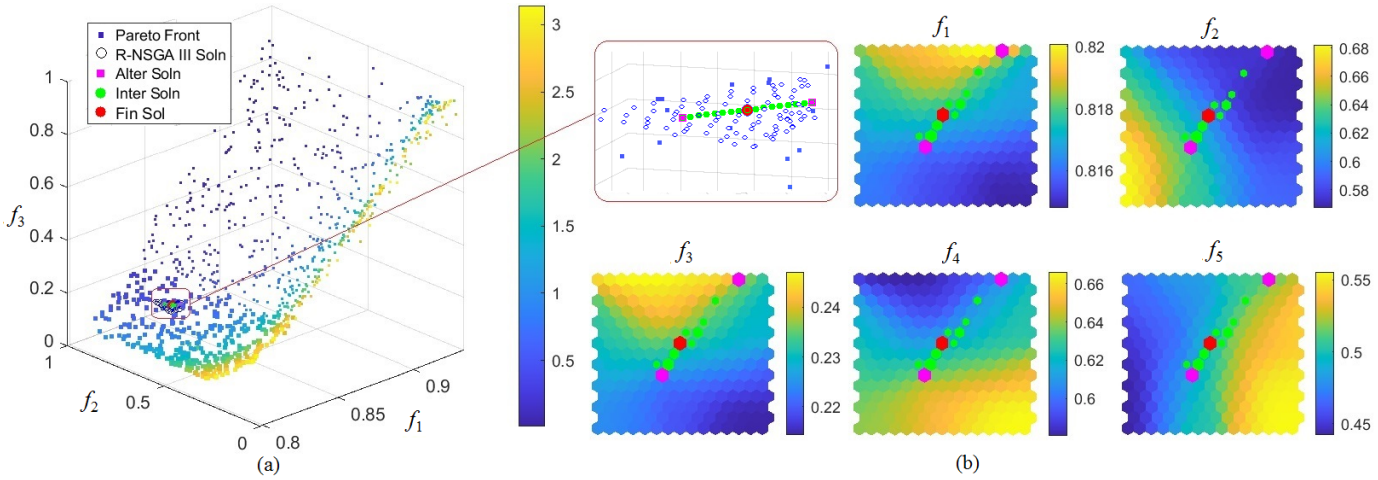


Fig. 10. WATER problem: (a) R-NSGA-III-obtained Pareto points and the NIMBUS solutions. (b) iSOM component planes of objectives using focused Pareto points and all critical NIMBUS points. The R-NSGA-III-obtained Pareto points in hollow blue markers are blown up for clarity.

are far away from the constraint boundary and also are at the boundary of the Pareto front, as can be confirmed from the scatter plot shown in Fig. 8(a). Choosing the two solutions on the selected part, 15 intermediate solutions (shown in green) are created in Step 9. Among these 15 solutions, the final solution, marked in red color, makes a good compromise in keeping f_1 and f_3 objectives not too worse, while forcing f_2 to go close to $\bar{z}_2 = 3.75$. The final solution is $\tilde{\mathbf{x}} = (0.50, 1.35, 1.29, 1.50, 2.11, 1.20, 0.40)$ with $\tilde{\mathbf{z}} = (33.293, 3.639, 11.640)$. It can be seen that this final solution is better than $\mathbf{z}^1$ in f_2 (reduced from 3.756 to 3.639) with slightly worse values in both f_1 (increased from 31.180 to 33.293) and f_3 (increased from 11.411 to 11.640). Although a desired target of $\bar{z}_2 = 3.75$ too close to $z_2^1 = 3.756$ was supplied in the classification step, the final solution has smaller value than $\bar{z}_2 = 3.75$, which is allowed.

B. WATER Problem

WATER problem has five objectives and seven constraints [41]. As discussed earlier, in order to visualize the near constraint violation Pareto optimal solutions, we compute the average of the normalized constraint violation and plot a separate component plane G using iSOM. Fig. 9(a) represents the scatter plot of the NSGA-III obtained Pareto front. Objectives f_1, f_2, and f_3 are represented on axes, f_4 is represented by marker size, and f_5 is represented on a color scale. Larger marker size and yellow marker color indicate the larger value of f_4 and f_5, respectively. This scatter plot is used only for verification purposes here. The NIMBUS solutions – start point, alternate solutions, intermediate solutions, selected and un-selected points after classification, near-constraint solutions, and the final solution are plotted on the scatter as well as the iSOM component planes. The start point is shown with a black cell. Clearly, iSOM component planes of objectives indicate that f_1 and f_3 are highly correlated, while others have trade-offs. Also, the start point is far away from the constraint boundary. The classification provided by the DM is shown below:

$$I^{<} = \{1, 3, 5\}, I^{\leqslant} = \varnothing, I^{\geqslant} = \varnothing, I^{=} = \varnothing, I^{<>} = \{2, 4\}.$$

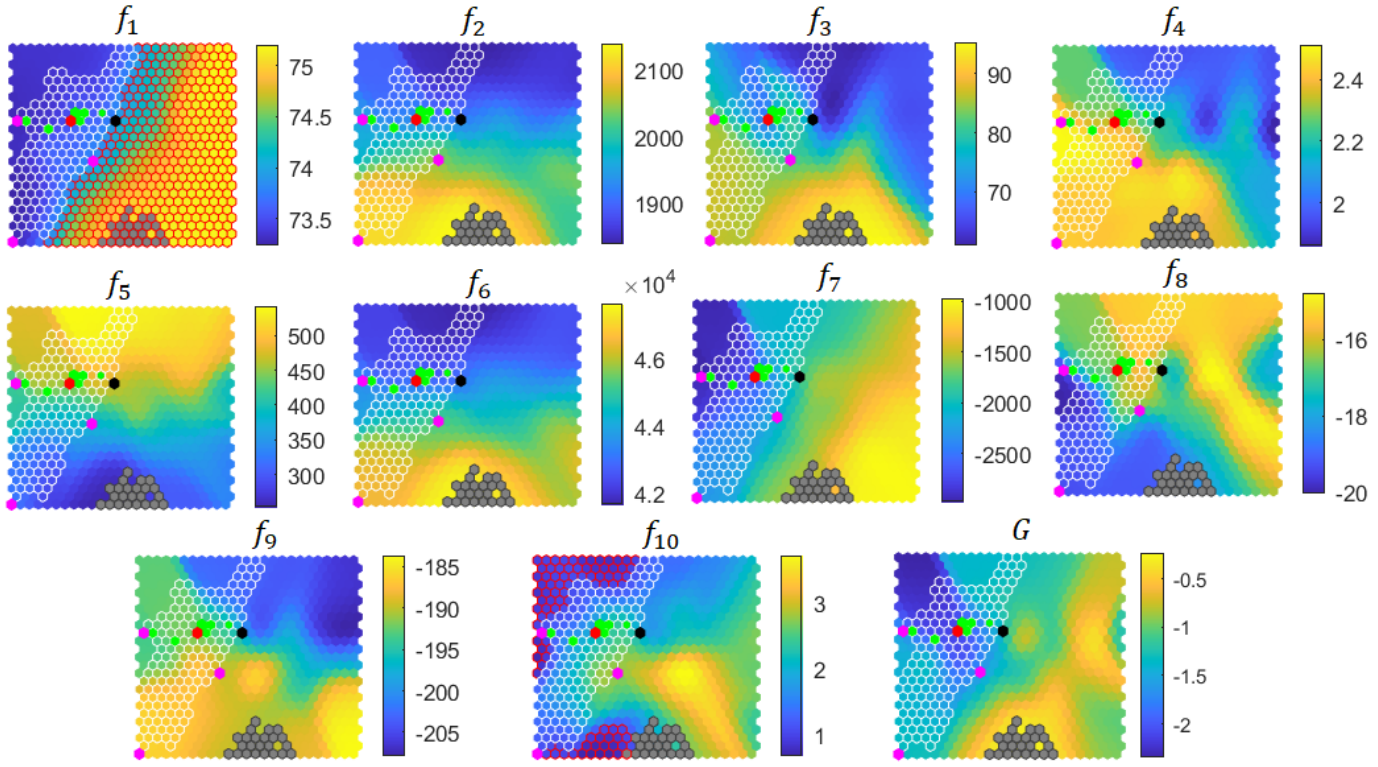


Fig. 11. GAA problem: iSOM component planes of objectives using complete Pareto points, selected and un-selected points after classification and all critical NIMBUS points- start point, alternate solutions, intermediate solutions and final solution.

DM wishes to improve f_1, f_3, and f_5 without any limit at the expense of possible worsening of f_2 and f_4 without any limit. Selected and un-selected cells are shown on iSOM component planes.

Three alternate solutions, marked with magenta color, are found by the NIMBUS procedure. The iSOM component planes make it clear that all three solutions lie on the selected part of the Pareto front and are far away from the constraint boundary. Also, it is clear that the alternate solutions do not unnecessarily make $I^{<>}$-class objectives too worse (not taking them to yellow cells) while improving $I^{<}$-class objectives slightly from the start point. The trade-offs in the objectives do not allow these alternate points to be away from each other.

To investigate the alternate solutions better, we apply R-NSGA-III using reference point $(0.817, 0.600, 0.232, 0.618, 0.499)$ and shrinkage factor of 0.1 to obtain more focused Pareto points. They are used to create a new set of iSOM-plots, which are shown in Fig. 10. Since the third alternate solution is relatively closer to the start point than the other two alternate solutions, hence for the given classification the third solution is worse than the other two alternate solutions. Therefore, the other two alternate solutions that are away from the start point are selected. 15 intermediate solutions are found using two chosen alternate solutions and are shown in green color. Eventually, the final solution, marked in red color, is found by observing a good compromise of intermediate solutions.

The final solution is $\tilde{\mathbf{x}} = (0.303, 0.024, 0.010)$ having $\tilde{\mathbf{z}} = (0.817, 0.600, 0.232, 0.618, 0.498)$. From the start point ($\mathbf{z}^1$) (see Table I in supplementary document), the final solution is better in f_1, f_3 and f_5 with a deterioration in f_2 and f_4, as desired by the classification. The use of iSOM-based visualization has helped in the process of arriving at the final solution by allowing the DM to have a comprehensive look at the entire Pareto set from its proximity to constraint boundary and objective trade-offs.

C. *GAA Problem*

General Aviation Aircraft (GAA) is a 10 objective problem [42] consisting of 27 decision variables and 18 constraints. A set of well converged Pareto optimal front has been generated using NSGA-II to plot the iSOM component plane of objective functions ($f_i;\ i = 1, \ldots, 10$) and average of normalized constraint violation (G) as shown in Fig. 11. From the iSOM component planes, the conflicting behaviour among the objective functions can be observed. The near CV solutions have been shown by grey color iSOM cells in objective functions and G component plane. After visualizing the near CV solutions, DM may wish to select a start point that is far from the region (grey color iSOM cells) having relatively larger near CV values. At the start point $\mathbf{z}^1$ = (73.87, 1885.35, 59.33, 1.97, 450.33, 42665.30, -2145.27, -15.33, -197.96, 1.08) (shown in black color cell in Fig. 11), the classification defined by the DM is-

$$I^{<} = \{1\}, I^{\leqslant} = \varnothing, I^{\geqslant} = \{10\}, I^{=} = \varnothing,$$

$$I^{<>} = \{2,\ 3,\ 4,\ 5,\ 6,\ 7,\ 8,\ 9\},$$

with $\varepsilon_{10} = 2.0$ to improve the objective function f_1 at the cost of f_{10} while letting freely change other objective functions.

Selected and un-selected region has been highlighted in iSOM component planes as per the color code defined in Table I. Upon solving the scalarized sub-problems, 3 different alternate solutions $\mathbf{z}^{1,1}, \mathbf{z}^{1,2}, \mathbf{z}^{1,3}$ have been obtained and plotted on iSOM component planes with magenta color cells. All the three alternate solutions are at boundary of the selected region obtained after classification step. Also, two out of three alternate solutions ($\mathbf{z}^{1,1}$ and $\mathbf{z}^{1,2}$) lies at the higher values of $f_2,\ f_3,\ f_4,\ f_6$ and f_9. So, DM decides to select an alternate solution that lies at higher values of f_4 and f_8 whereas relatively lower values of other objectives. Next, 15 intermediate solutions has been generated between the start point $\mathbf{z}^1$ and selected alternate solutions $\mathbf{z}^{1,3}$ that has been shown with green color iSOM cells. The final solution $\tilde{\mathrm{z}}$ = (73.28, 1928.23, 76.16, 2.42, 464.41, 43117.99, -2675.36, -16.36, -193.18, 1.98), has been selected amongst the intermediate solutions that is a trade-off solution amongst all the objective functions. The final solution ($\tilde{\mathrm{z}}$) has improved the value of the objective function f_1 from 73.87 to 73.28 by deteriorating the value of objective function f_{10} from 1.08 to 1.98, while letting other objectives change freely. Therefore, iSOM visualization aids the decision maker to select the alternate solution that has lower f_1 values and trade-off values for other objectives.

VIII. Conclusions

Visualization of Pareto-optimal solutions in terms of their proximity to constraint boundaries, cluster boundaries, trade-off among objectives, etc. are vital for the decision-makers (DMs) to execute multi-criterion decision-making (MCDM) procedure to arrive at a preferred solution. The usual visualization methods used in MCDM activities, such as the parallel coordinate plots, radial visualization, scatter plots, etc. are not adequate to have a clear insight into the above properties of high-dimensional Pareto solutions. In this paper, we have proposed an interpretable self-organizing map (iSOM) approach which makes two-dimensional maps of each objective and constraint violation functions from Pareto solutions to provide a comprehensive picture. We have briefly discussed the iSOM approach and indicated how the original NIMBUS decision-making procedure can be aided with iSOM component planes. We have proposed a color and style scheme for visualizing each cell of iSOM to clearly show (i) cells with function-value based coloring, (ii) near-constraint cells, (iii) the starting cell, (iv) cells that satisfy (and do not satisfy) NIMBUS classification of objectives, (v) alternate NIMBUS-obtained solutions meeting classification conditions, (vi) created intermediate solutions from a chosen set of alternate solutions, and (vii) the final solution. iSOM component planes can help DMs to make decisions in most of their steps by visualizing two-dimensional iSOM component planes. For clarity, the procedure has been aided with creating iSOM component planes with focused Pareto points obtained using R-NSGA-III procedure at the preferred part of the Pareto front.

The iSOM-NIMBUS procedure has been demonstrated on a number of constrained and unconstrained numerical problems and real-world problems from three to five-objective problems. The detail description of the plots has helped to understand the NIMBUS procedure better and importantly has demonstrated how iSOM visualization with points, either from the complete Pareto set or from a part of the Pareto set, has been able to provide a more informed decision-making aid to the use of the NIMBUS procedure.

The iSOM visualization methodology is now ready to be used with other MCDM procedures, such as Pareto race [18], [19], STOM [17], GUESS [16] and other methods [1]. A layered iSOM approach in which higher-level iSOM cells can be expanded with lower-level iSOM cells in a continuous manner can be implemented to focus on larger to smaller areas on the Pareto front. Focused EMO procedures, such as R-NSGA-III [36], must be run quickly using a parallel computing environment to enable such transitions smoothly. Other key features of Pareto solutions, such as knee points having large trade-off among objectives [38], [39], holes, robust solutions against uncertainties, etc. can also be implemented in the iSOM approach for easy visualization. Nevertheless, this paper has shown the importance of bringing multi-criterion optimization and multi-criterion decision-making tasks closer together and demonstrated that the proposed iSOM approach can aid in making informed decisions at various stages of the decision-making process by providing DMs a clearer and deeper understanding of the Pareto solutions.

References

1 Miettinen, K., "Nonlinear multiobjective optimization," in *International series in operations research and management science*, 1998.

2 Steuer, R. E., "Multiple criteria optimization," *Theory, computation and applications*, 1986.

3 Chankong, V. and Haimes, Y. Y., *Multiobjective decision making: theory and methodology*. Courier Dover Publications, 2008.

4 Deb, K., *Multi-Objective Optimization using Evolutionary Algorithms*. John Wiley & Sons, 2001.

5 Coello, C. A. C., Lamont, G. B., Van Veldhuizen, D. A. *et al.*, *Evolutionary algorithms for solving multi-objective problems*. Springer, 2007, vol. 5.

6 Deb, K. and Jain, H., "An evolutionary many-objective optimization algorithm using reference-point-based nondominated sorting approach, part i: Solving problems with box constraints," *IEEE Transactions on Evolutionary Computation*, vol. 18, no. 4, pp. 577–601, 2014.

7 Zhang, Q. and Li, H., "Moea/d: A multiobjective evolutionary algorithm based on decomposition," *IEEE Transactions on evolutionary computation*, vol. 11, no. 6, pp. 712–731, 2007.

8 Ma, J., Fan, Z.-P., and Huang, L.-H., "A subjective and objective integrated approach to determine attribute weights," *European journal of operational research*, vol. 112, no. 2, pp. 397–404, 1999.

9 Branke, J., Greco, S., Słowiński, R., and Zielniewicz, P., "Interactive evolutionary multiobjective optimization using robust ordinal regression," in *International conference on evolutionary multi-criterion optimization*. Springer, 2009, pp. 554–568.

10 Sinha, A., Korhonen, P., Wallenius, J., and Deb, K., "An interactive evolutionary multi-objective optimization algorithm with a limited number of decision maker calls," *European Journal of Operational Research*, vol. 233, no. 3, pp. 674–688, 2014.

11 Wierzbicki, A. P., "The use of reference objectives in multiobjective optimization," in *Multiple criteria decision making theory and application*. Springer, 1980, pp. 468–486.

12 Wierzbicki, A., "Reference point approaches," in *Multicriteria decision making*. Springer, 1999, pp. 237–275.

13 Miettinen, K., *Nonlinear multiobjective optimization*. Springer Science & Business Media, 2012, vol. 12.

14 Hall, W. A. and Haimes, Y. Y., "The surrogate worth trade-off method with multiple decision-makers," in *Multiple criteria decision making Kyoto 1975*. Springer, 1976, pp. 207–233.

15 Shimizu, K., Kawabe, H., and Aiyoshi, E., "A theory for interactive preference optimization and its algorithm-generalized swt method," *The Transactions of the Institute of Electronics and Communication Engineering of Japan*, vol. 61, pp. 1075–1082, 1978.

16 Buchanan, J. T., "A naive approach for solving mcdm problems: The guess method," *Journal of the Operational Research Society*, vol. 48, no. 2, pp. 202–206, 1997.

17 Nakayama, H. and Sawaragi, Y., "Satisficing trade-off method for multiobjective programming," in *Interactive decision analysis*. Springer, 1984, pp. 113–122.

18 Korhonen, P. and Wallenius, J., "A pareto race," *Naval Research Logistics (NRL)*, vol. 35, no. 6, pp. 615–623, 1988.

19 Korhonen, P. and Yu, G. Y., "Quadratic pareto race," in *New Frontiers of Decision Making for the Information Technology Era*. World Scientific, 2000, pp. 123–142.

20 Deb, K. and Abhishek, K., "Interactive evolutionary multi-objective optimization and decision-making using reference direction method," in *Proceedings of the 9th annual conference on Genetic and evolutionary computation*, 2007, pp. 781–788.

21 Deb, K. and Kumar, A., "Light beam search based multi-objective optimization using evolutionary algorithms," in *2007 IEEE Congress on Evolutionary Computation*. IEEE, 2007, pp. 2125–2132.

22 Jaszkiewicz, A. and Słowiński, R., "The 'light beam search'approach–an overview of methodology applications," *European Journal of Operational Research*, vol. 113, no. 2, pp. 300–314, 1999.

23 Kadziński, M., Tomczyk, M. K., and Słowiński, R., "Preference-based cone contraction algorithms for interactive evolutionary multiple objective optimization," *Swarm and Evolutionary Computation*, vol. 52, p. 100602, 2020.

24 Tomczyk, M. K. and Kadziński, M., "Robust indicator-based algorithm for interactive evolutionary multiple objective optimization," in *Proceedings of the Genetic and Evolutionary Computation Conference*, 2019, pp. 629–637.

25 Miettinen, K. and Mäkelä, M., "Interactive bundle-based method for nondifferentiable multiobjeective optimization: Nimbus," *Optimization*, vol. 34, no. 3, pp. 231–246, 1995.

26 Nagar, D., Ramu, P., and Deb, K., "Interpretable self-organizing maps (isom) for visualization of pareto front in multiple objective optimization," in *Evolutionary Multi-Criterion Optimization*. Cham: Springer International Publishing, 2021, pp. 645–655.

27 Miettinen, K., Ruiz, F., and Wierzbicki, A. P., *Introduction to Multiobjective Optimization: Interactive Approaches*. Berlin, Heidelberg: Springer Berlin Heidelberg, 2008, pp. 27–57. [Online]. Available: https://doi.org/10.1007/978-3-540-88908-3_2

28 Miettinen, M., *Comparative Evaluation of Some Interactive Reference Point-based Methods for Multi-Objective Optimisation*. Journal of the Operational Research Society, 1999, vol. 50, pp. 949–959.

29 Miettinen, K. and Mäkelä, M., "Nimbus — interactive method for nondifferentiable multiobjective optimization problems," 01 1996.

30 Miettinen, K. and Marko, M., "Synchronous approach interactive multiobjective optimization," *European Journal of Operational Research*, vol. 170, pp. 909–922, 05 2006.

31 Miettinen, K. and Mäkelä, M. M., "On scalarizing functions in multiobjective optimization," *OR Spectrum*, vol. 24, pp. 193–213, 2002.

32 Deb, K. and Miettinen, K., "Nadir point estimation using evolutionary approaches: better accuracy and computational speed through focused search," in *Multiple criteria decision making for sustainable energy and transportation systems*. Springer, 2010, pp. 339–354.

33 Kohonen, T., "Exploration of very large databases by self-organizing maps," *Proceedings of International Conference on Neural Networks (ICNN'97)*, vol. 1, pp. PL1–PL6 vol.1, 1997.

34 Thole, P., "Design space exploration and optimization using self-organizing maps," *Struct Multidisc Optim 62, 1071–1088*, 2020.

35 Deb, K. and Sundar, J., "Reference point based multi-objective optimization using evolutionary algorithms," in *Proceedings of the 8th annual conference on Genetic and evolutionary computation*, 2006, pp. 635–642.

36 Vesikar, Y., Deb, K., and Blank, J., "Reference point based nsga-iii for preferred solutions," in *2018 IEEE Symposium Series on Computational Intelligence (SSCI)*, 2018, pp. 1587–1594.

37 Miettinen, M., *Interactive Multiobjective Optimization System WWW-NIMBUS on the Internet*. Computers & Operations Research, 2000, vol. 27, pp. 709–723.

38 Talukder, A. K. A. and Deb, K., "Paletteviz: A visualization method for functional understanding of high-dimensional pareto-optimal data-sets to aid multi-criteria decision making," *IEEE Computational Intelligence Magazine*, vol. 15, no. 2, pp. 36–48, 2020.

39 Deb, K. and Talukder, A. K. A., "Visualization-based multi-criterion decision making with nimbus method using palette viz," in *2021 IEEE Symposium Series on Computational Intelligence (SSCI)*. IEEE, 2021, pp. 1–8.

40 Li, K., Omidvar, M. N., Deb, K., and Yao, X., "Variable interaction in multi-objective optimization problems," in *Parallel Problem Solving from Nature – PPSN XIV*. Cham: Springer International Publishing, 2016, pp. 399–409.

41 Deb, K., Pratap, A., Agarwal, S., and Meyarivan, T., "A fast and elitist multiobjective genetic algorithm: Nsga-ii," *IEEE Transactions on Evolutionary Computation*, vol. 6, no. 2, pp. 182–197, 2002.

42 Simpson, T., Allen, J., Chen, W., and Mistree, F., "Conceptual design of a family of products through the use of the robust concept extrapolation method," in *6th Symposium on Multidisciplinary Analysis and Optimization*, 1996, p. 4161.